EAI Endorsed Transactions
on Industrial Networks and Intelligent Systems
Research Article EAI.EU

A compact 1 × 3 two-mode selective silicon photonic router/switch using two tunable phase shifters

Duong Quang Duy[1*], Truong Cao Dung[1], Dang Hoai Bac[1], Nguyen Binh[1], Nguyen Tan Hung[2], Tang Tan Chien[3], Le Thi Phuong Mai[3], Nguyen Vy Rin[2], Phan Thi Thanh Van[2]

[1]Posts and Telecommunications Institute of Technology, Vietnam
[2]The University of Danang - Advanced Institute of Science and Technology, Vietnam
[3]The University of Danang - University of Science and Technology, Vietnam

Abstract

In this work, we propose a design in the proof-of-concept of a 1×3 two-mode selective silicon-photonics router/switch. The proposed device composes of a Y-junction coupler, two multimode interference (MMI) couplers, and two phase-shifters on the silicon-on-insulator (SOI) rib waveguides. The input modes of TE_0 and TE_1 can be arbitrarily and simultaneously routed to the yearning output ports by setting appropriate values (ON/OFF) for two tunable phase shifters (PSs). The structural optimization and efficient characterization processes are carried out by numerical simulation via three-dimensional beam propagation method. The proposed device exhibits the operation ability over the C-band with good optical performances in terms of insertion loss smaller than 1 dB, crosstalk under -19 dB, and relatively large geometry tolerances. Moreover, the proposed device can integrate into a footprint as compact as 5 μm × 475 μm. Such significant advantages are beneficial and promising potentials for very large-scale photonic integrated circuits, high-speed optical interconnects, and short-haul few-mode fiber communication systems.

Received on 30 July 2021; accepted on 13 September 2021; published on 17 September 2021

Keywords: mode division multiplexing, silicon-on-insulator, multimode interference waveguides, Y-junction coupler, mode multiplexing switch.

doi:10.4108/eai.17-9-2021.170962

1. Introduction

Recently, multimode division multiplexing (MDM) has received remarkable consideration due to its superior capacity for short-reach optical fiber communication systems, photonics on-chip interconnects, and photonic computing systems [1–3]. By combination between the MDM technique and the wavelength division multiplexing (WDM) technique on a merged platform, we can attain a multifold increase of the aggregated channel capacity, because various orthogonal mode division signals from the MDM channels can share a specific wavelength without the impacts of inter-frequency crosstalk and nonlinearity. Typically, multimode fibers using in MDM communication systems only support a relatively small number of guided modes which are thus called few-mode fibers because a large number of guided modes cause degraded signals from high-order and inter-modal dispersion issues associated with nonlinear effects [4, 5]. However, and silicon crystals in the silicon waveguide, hybrid WDM-MDM systems are still able to apply for short-haul optical communication systems [6–9] and optical interconnects [10–12] thanks to the support of advanced dispersion compensation techniques [13, 14]. Basically, technology developers typically use graded-index fibers optimized for minimum differential modal group delay (DMGD) because such fibers allow the use of simpler receiver technology. However, in principle, we can use step-index fibers such as few-mode fibers to connect to an MDM chip due to the high coupling efficiency between a few-mode fiber and a planar few-mode waveguide [15, 16].

Besides, currently, an on-chip MDM system, especially CMOS-compatible silicon-based MDM systems, is preferable to provide a possible way for the large-scale high-capacity data exchange in data communication

*Corresponding author. Email: duydq@ptit.edu.vn

networks (DCNs) [17] due to utilizing significant highlights of silicon photonics, such as high compactness, low loss, broad-spectrum response, reasonable manufacturing cost. Silicon photonics-based MDM devices also play the important roles to construct chip-scale systems through many photonic mode division signal processing functionalities, such as mode (de)multiplexing [18–21], mode add/drop multiplexing [22, 23], mode conversion [24, 25], mode routing [26, 27], and mode switching [28–31]. It is seen that since the thermo-optic (TO) effect has been widely applied to control the phase angle of light when traveling through the silicon waveguides [31, 32], the MDM devices based on the SOI platform could operate much more flexibly via the phase-driven process by manipulating metallic microheaters. Researchers on MDM devices meet a good chance to invent as a farmer found a fertile field for sowing. For instance, a lot of reconfigurable MDM devices based on silicon photonic which are demonstrated in fact [32–38] or numercially simulated [39, 40] can be configured quickly by using the thermo-optic conductive microheaters.

Among various functional MDM devices, currently, the conventional mode (de)multiplexers are being renovated to become the simultaneous mode-selective routers by introducing the switchable functionality which is implemented via controllable phase shifters based on thermal-optically conductive microheater [32, 33, 39, 40]. That means, we can integrate the switchable functionality into the mode (de)multiplexers in order to realize the mode exchanging and routing functions. Such investigations are paying attention to the silicon photonics community because they can give an enhancement for the feasible and flexible all-photonic complexity signal processing functionalities. However, some recent innovative investigations on two-mode selective routers are existing some drawbacks due to needing many cascaded and tailed sections or many tunable phase shifters thus leading to a relatively large size or a highly electrical power consumption.

In this paper, we introduce a proof-of-concept design of a compact 1 × 3 mode selective switch/router for two modes TE_0 and TE_1 based on the SOI material platform which utilizes a Y-junction coupler, and two multimode interference couplers, and two tunable phase shifters (PSs) controlled by two states (ON and OFF). We choose the design for two lowest order modes of transverse electric (TE) modes because they are two modes guided in silicon waveguides possessing lowest cutoff frequencies and so-called the dominant modes. In general, only the dominant mode has a sinusoidal dependence upon distance and thus possesses fields that are periodic in the wave propagating space. This structure is simpler or supports more output ports than that of the previous publications [31, 32, 36]. By using the numerical simulation methods, including

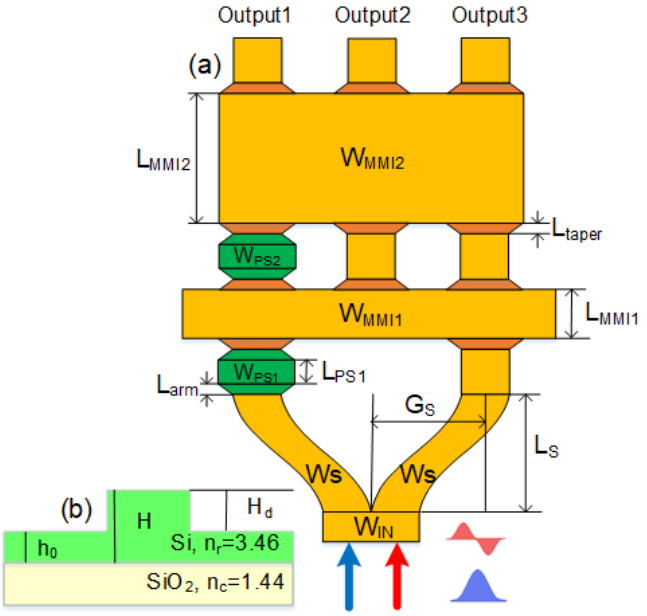

Figure 1. The schematic diagram of the proposed mode switch: (a) top view ; (b) side view.

beam propagation method (BPM) and effective index method (EIM), from Rsoft's commercial simulation tools with the sufficient enough grid sizes of Δx= Δy= Δz= 1 nm for the whole device, we show that the proposed switch/router can be an arbitrary mode exchange and arbitrary mode selective router from two input modes of TE_0 and TE_1 to optional three output ports by setting suitable phase difference values for two tunable phase shifters. Furthermore, the device also verifies low insertion loss levels (> - 1 dB), relatively small crosstalk (< - 19 dB) levels, and relatively low fabrication tolerances over the C band.

2. Structure design and optimization

2.1. General description

Fig. 1 illustrates a schematic diagram in the proof-of-concept of 1 × 3 two-mode selective switch/router. It comprises a symmetrical Y-junction coupler, a 2 × 3 multimode interference (MMI) coupler, and a 3 × 3 MMI coupler. This designed structure is equipped with two tunable phase shifters (PSs). The function of the Y-junction coupler is to equally split the input signals to branched waveguides and convert the optical modes to fundamental mode (TE_0). The first MMI coupler is to straightforwardly guide two optical fields, which are transmitted from two arms of the Y-junction coupler or combine into a unique field at the central line of the first MMI coupler following the suitable phase difference from the first tunable phase shifter. Whereas, the second MMI coupler plays the role of a mode combiner to desired outputs through interference

mechanisms according to the suitable phase difference of the second tunable phase shifters. To improve the coupling efficiency, tapered waveguides are inserted into output ports of MMI couplers before connecting to access waveguides. Design and optimization processes of the whole device are carried out via the 3D-BPM simulation method incorporated into the effective index method.

The proposed device is embedded into the rib/ridge waveguides from a standard SOI wafer. As shown in Fig. 1(b), the heights of the silicon layer and the slab layer are initially chosen corresponding to 220 nm and 120 nm, respectively. In this paper, the refractive index of Si is as equal as 3.46 and the refractive index of SiO_2 is equal as 1.444 at the wavelength of 1550 nm which are determined from the reference [41, 42]. To optimize the device, we utilize the beam propagation method (BPM) and the effective index method (EIM) together [43]. The device is also designed to support the operation of only two lowest-order TE modes.

2.2. Y-junction coupler

The 1 × 2 Y-junction coupler operates as an ideal optical power splitter, and transform guided modes to TE_0 modes at the outputs. The input lights are divided equally at two output waveguides with the same phase for TE_0 input light and out of phase for TE_1 one [44]. The structure of the Y-junction coupler begins with a stem waveguide having a width W_{IN}. This width is large enough to support the propagation for both modes of TE_0 and TE_1. To find out the beneficial width of the stem waveguide, we use numerical simulations to investigate the refractive indices of TE modes [45]. By employing the mode solver tool, we obtain the refractive index of guided modes as a function of the stem waveguide W_{IN}, as exhibited in Fig. 2. From the calculated diagram of effective indices of TE modes following the variation of the input stem width of the Y-junction, we select W_{IN} = 1.2 μm at the cutoff point where the device can support only two guided modes TE_0 and TE_1.

The Y-junction waveguide divides the optical guided modes into two ideal fields at two symmetrically branched waveguides, possessing the vertical length L_S and horizontal width G_S. The width of each branched waveguide is W_S, which is dedicated to guiding only the fundamental modes. Two branched waveguides of Y-junction are the sinusoidal waveguides so-called S-bent waveguides because they are beneficial for reducing the power loss at a large enough radius[46, 47]. In this design, we optimized the geometric structure of the symmetric Y-junction to reach an acceptable transmission efficiency when it acts in the role of an ideally optical splitter. It is well-known that when a field $\Psi(x, z)$ is introduced in the Y-junction length of L_{IN}

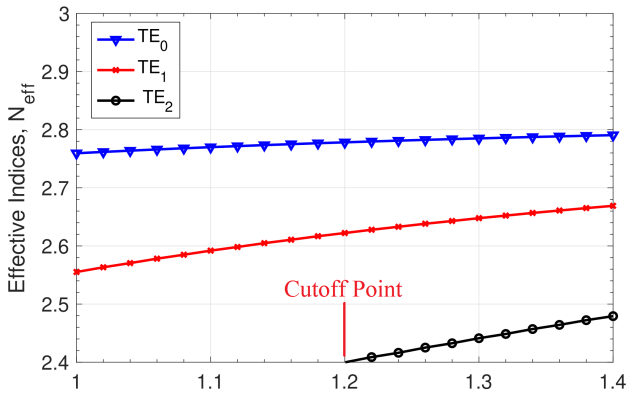

Figure 2. The simulated diagram of effective indices of two TE modes as functions of the the input stem waveguide width.

and width of W_{IN}, the output field can be estimated as [44]:

$$\Psi(W_{IN}, L_{IN}) = \sum_{m=1}^{2} \varepsilon_{m\nu} \int_0^{Ls} \phi_{m\nu}(x, z)dz, \qquad (1)$$

where m is the order number of the coupler branches, ν is the mode-grade index of each eigenmode, and $\varepsilon_{m\nu}$ is called the power-excited-coefficient of each mode per each branch.

In our design, two branches of the Y-junction has the same width $W_S = W_{IN}/2$ (Fig. 1). We need to find an optimal value of the length L_S of the Y-junction coupler. This process can be done via numerical simulations. To this end, we set $C_{m\nu} = |\varepsilon_{m\nu}|^2$ and investigate L_S with respect to each mode TE_0/TE_1. Fig. 3 shows that the behavior of TE_0 power excitation is significantly different from that of TE_1 mode. Particularly, the power excitation coefficient of TE_0 fluctuates strongly from an approximate portion from 44.46 % to 44.62 %, while the

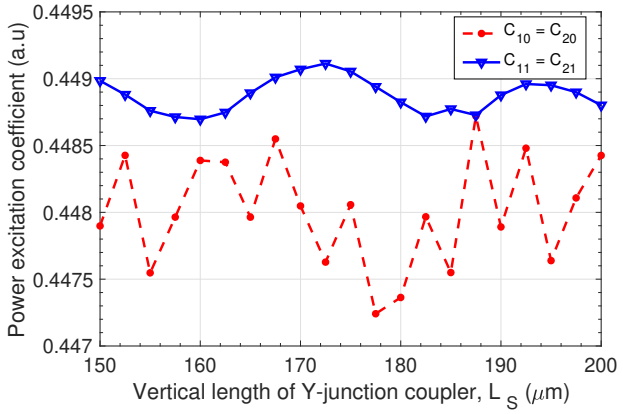

Figure 3. Power excitation coefficients of the TE modes as functions of the length L_S of the Y-junction coupler.

similar coefficient of TE_1 mode varies slightly around 44.58 %. To achieve a balanced power between the two modes, we selected L_S = 187 μm as the optimal length of the Y-junction coupler.

2.3. 2 × 3 MMI coupler (MMI_1)

As can be seen in Fig. 1, two output waveguides of the Y-junction coupler are connected to a 2 × 3 MMI coupler (MMI_1), which is characterized by a width W_{MMI_1} and a vertical length L_{MMI_1}. The two input waveguides of MMI_1 coupler are placed at the positions of $\pm W_{MMI_1}/4$, while the middle output waveguide is located right at the center of MMI_1. To obtain the desired switching functionality, MMI_1 is designed to exhibit symmetric interference mechanisms [48]. It means that if the two input lights are in phase, the lights will be combined and directed to the center output port of MMI_1. Meanwhile, if the two input lights are out of phase, the lights will be straightforward to outer arms of MMI_1, respectively. These mechanisms will well operate in principle if the length of MMI_1 satisfies the following condition:

$$L_{MMI_1} = \frac{m}{4n} 3L_\pi, \tag{2}$$

where m and n are integers with m is the number of interference periods, n is the number of single images and L_π is half-beat length of the MMI_1 coupler, given by

$$L_\pi = \frac{4n_e W_{\text{eff}}^2}{3\lambda}, \tag{3}$$

where λ is the operating wavelength, n_e is the effective refractive index of the core. Here W_{eff} is the effective width of W_{MMI_1}, defined by [48]

$$W_{\text{eff}} = W_{MMI_1} + \frac{\lambda}{\pi}\left(n_e^2 - n_c^2\right)^{-\frac{1}{2}}, \tag{4}$$

where n_c is the refractive index of cladding layer.

In the case of TE_0 mode led, to make the device length minimum, we apply eq. (2) with $m = 1$ and $n = 2$. Through numerical simulations around $L_{MMI_1} = 3L_\pi/8$, the optimal values for W_{MMI_1} and L_{MMI_1} are found at 6.8 μm and 43 μm respectively to obtain the smallest insertion loss at the outputs of MMI_1.

2.4. 3 × 3 MMI coupler (MMI_2)

Three input ports of the MMI_2 coupler are then connected directly to the output ports of MMI_1 as shown in Fig. 1. To attain desirable functions, MMI_2 is designed to operate the general interference mechanism of 2 × 2 MMI [48]. It means that MMI_2 will work as a 3-dB coupler when the lights are injected to two outer input ports with a phase difference of $\pm\ \pi/2$. Meanwhile, the light injected through the center input port will be reproduced to the central output port of MMI_2 since it has also performed the symmetric interference mechanism of 1 × 1 MMI with $m = 2$ and $n = 1$ [48]. Therefore, the length of MMI_2 is determined to be $L_{MMI_2} = 3L_\pi/2$. Through the optimization process by the numerical simulation BPM, the optimal values of L_{MMI_2} and W_{MMI_2} are respectively found at 98 μm and 5 μm in order to obtain the highest transmission efficiency for MMI_2.

2.5. Phase shifters (PS)

As we all know that the shifted phase of a mode field when passing through an optical waveguide does not only depend on the width of the waveguide but also depends on its effective refractive index N_{eff} [25] as expressed in (5) by L. Soldano [40, 48]. In order to demonstrate the proof-of-concept of the proposed device, we consider the dependence of such the phase angle on the variation of PS's effective index under the impact of temperature [41]. This effect is called the thermo-optic effect. For instance, heaters adjusted by external voltages may cause the refractive index change N_{eff} of the core silicon layer [49]. The evolution phase angle change propagating through a silicon waveguide with the variable width can be calculated by the following relation [25]:

$$\begin{aligned}\Phi(0, L_{\text{PS}}) &= \int_0^{L_{\text{ps}}} (\beta_0(z) - \beta_v(z))dz, \\ &\approx \frac{3\pi\lambda}{4} \int_0^{L_{\text{ps}}} \frac{dz}{N_{\text{eff}} W_{\text{ps}}^2(z)},\end{aligned} \tag{5}$$

where L_{PS} and W_{PS} are the central length and the central width of PS (as seen in Fig. 1), β_0 and β_v are propagation constants of the mode fields with v being the order index of a guided mode.

Based on the working principle of the symmetric Y-junction coupler, we classify the PS_1 states into two control states: ON and OFF. We set the ON-state to make the injected mode of TE_1 traveling through the Y-junction and MMI_1 to the central output of MMI_1, whereas OFF-state is when the TE_0 mode is diverted to this output of MMI_1. To find out the necessary phase shift for switching, we look into the N_{eff} of PS_1 relating to two the control states [49]. First, we experientially choose the dimension values of the PS_1. Then, we excite the mode TE_0 at the input of the Y-junction and investigate the phase difference between the outputs of two branches as a function of N_{eff} within the range of [2.77, 2.78]. From the investigation plotted in Fig. 4a, we obtain $N_{\text{eff}_1} = 2.747$ and $N_{\text{eff}_2} = 2.775$ corresponding to OFF and ON control states of PS_1, respectively. In our design, the phase difference caused by the variation in the width of PS_1, and investigated as a function of W_{PS_1} in Fig. 4b. The W_{PS_1} width is found at 0.9 μm and

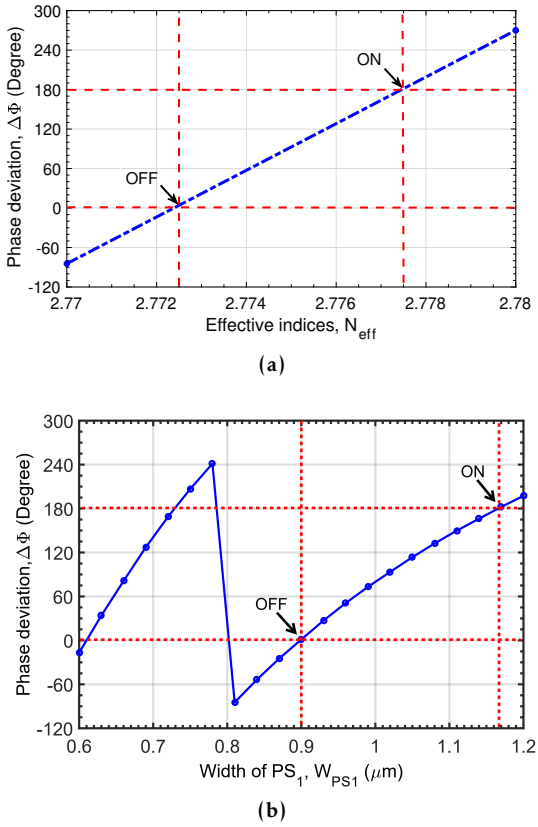

Figure 4. Phase difference between two branches of the Y-junction as a function of : a) the effective indices, N_{eff}; b) the PS_1 width, W_{PS_1}.

Table 1. Control states to two PSs to realize the switching functionalities of the device for all configurations.

Input modes	Output ports	State of PS_1	State of PS_2
TE_0/TE_1	O_2/O_3	OFF	OFF
	O_2/O_1	OFF	ON
	O_1/O_2	ON	ON
	O_3/O_2	ON	OFF

1.16 μm for the OFF-state and ON-state, respectively. Otherwise, the PS_2 only works well when it is designed to make a phase deviation of $\pm\,\pi/2$ [6]. In order to use such conditions of control states ON and OFF of PS_1 for PS_2, the phase difference of guided mode before working through PS_2 has to be shifted a angle of $\pm\,\pi/2$. To do this work, we investigated the width of the W_{S_2} which close to PS_2 (instead of $W_S = 0.6\ \mu$m chosen above). The investigated result in Fig. 5 shows that, the light will be shifted a phase angle of $-\,\pi/2$ at $W_{S_2} = 0.657\mu$m before entering into PS_2. Therefore, when the PS_2 in OFF state (zero radians), the guided mode needs to be shifted a quantity of $-\,\pi/2$ before propagating the

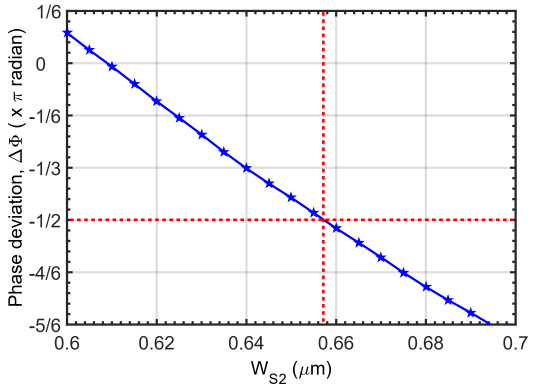

Figure 5. Phase difference as a function of W_{S_2}.

MMI_2. Alternatively, when PS_2 in ON state (π radian), this phase angle is equal to $\pi/2$. Consequently, two guided modes in two cases are led to two individual outer arms of the MMI_2. Otherwise, in the rest cases for both TE_0 and TE_1, guided modes are traveled to the central output port of this MMI after passing through a center output port of the MMI_1 in principle with the symmetric interference mechanism [6].

As a result, all required working states of the proposed device can list in Table 1. One can see that TE_0 and TE_1 modes are always selectively routed to three different outputs of the designated device when simultaneously injecting into the input.

3. Performance Evaluation and Discussions

To realize and indicate feasible functions of the proposed structure, numerical simulation of BPM has been manipulated to demonstrate the operation ability in the proof-of-concept. First, we are interested in the visual electric-field pattern observation of the optical guided modes from the input port to output ports. Fig. 6 (g)-(h) shows the electric-field patterns of TE_0 and TE_1 modes at the 1550 nm wavelength. Their revolutions for all happenable cases of guided modes in Fig. 6 (a)-(f) can be briefly summarized in Table 1 that are true with the theoretically analyzed results. The upper and lower rows of Fig. 6 (a)-(f) successively show the exciting fields at the input port corresponding to TE_0 and TE_1 modes, respectively. The color bar on the right side of Fig. 6 indicates the normalized field intensity. Such six states fulfill enough cases for operation states of the proposed device, as listed in Tab. 1. One can see that distributed optical fields in all cases are clear and acceptable in our design and optimization. As shown in Fig. 6 (a)-(f), one may observe that a small number of optical power fractions of the guided modes have radiated to the outside or leaked to the cladding layers when propagating from the input port to the output ports. and inavoidable crosstalk in the multimode regions.

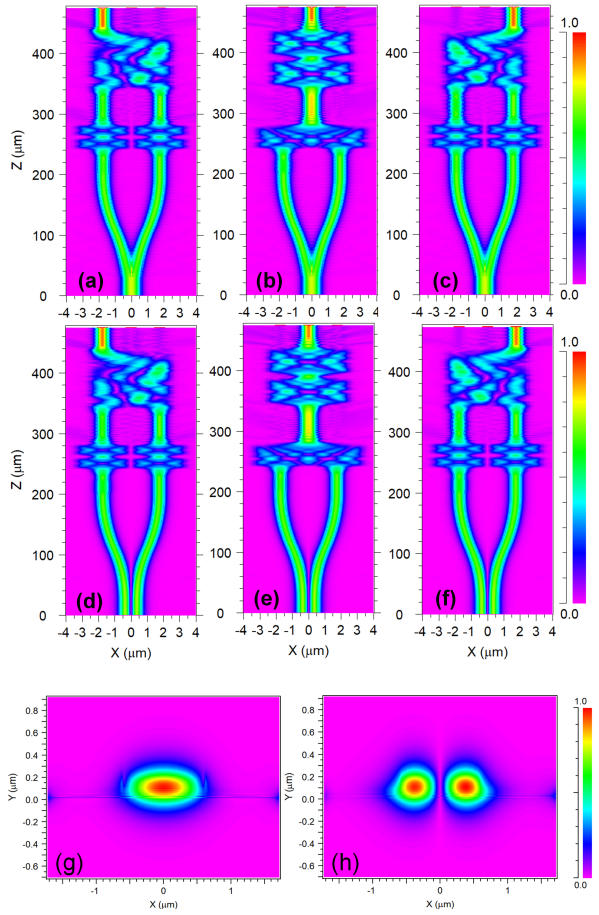

Figure 6. Electric field patterns for TE_0 mode (a-c) and TE_1 (d-f) to three different outputs, Contour maps of electric field distributions at input modes (g) TE_0 and (h) TE_1. The color bars indicate the normalized field intensity.

To further characterize the optical performances of the suggested device, we introduce two indispensable specific parameters composing of insertion loss (I.L) and crosstalk (Cr.T), which are defined by the following expressions:

$$\text{I.L} = 10\log_{10}\left(\frac{P_{\text{out}}}{P_{\text{in}}}\right)[dB], \tag{6}$$

$$\text{Cr.T} = -10\log_{10}\left(\frac{P_{\text{out}}}{P_{\text{disregarded}}}\right)[dB], \tag{7}$$

where P_{in} is the injected power at the device input, P_{out} is the optical power at a yearned output, $P_{\text{disregarded}}$ is the disregarded power propagating to a yearned output port. I.L has a relation to the total lossy power portions out of the device, Cr.T is the total crosstalked power fractions from disregarded output ports associating with a yearned output port.

In this section, we will characterize the optical performances including I.L and Cr.T for the proposed switch, corresponding to configurations of TE_0 and TE_1

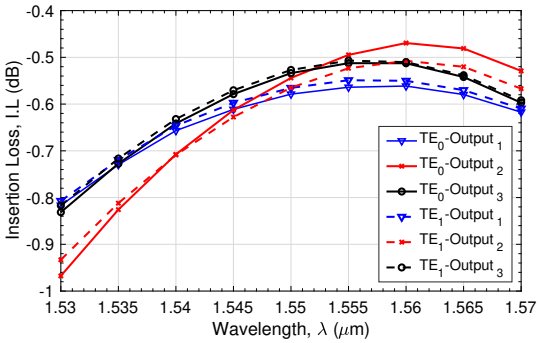

(a) Insertion loss

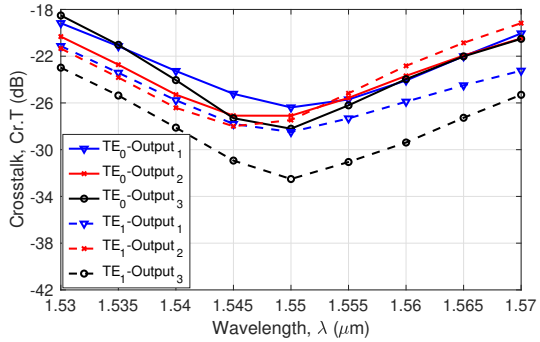

(b) Crosstalk

Figure 7. Insertion loss (a) and crosstalk (b) of the proposed switch as a function of the operation wavelength for TE_0 and TE_1 modes at three outputs

listed in Table 1 (Figs. 7-11). Figures 7a and 7b illustrate the characterization curves of I.L and Cr.T as functional variations of the wavelength. The operating wavelength range is surveyed from 1530 *n*m to 1570 *n*m. It can be seen that I.L of all cases increase gradually from 1530*n*m at - 0.97 dB, get peak approximately - 0.47 dB at the wavelength range λ =1555 nm-1565 nm, then drop gradually and end at the value of - 0.62 dB at λ=1570 nm. Besides, in the mentioned wavelength range, I.L of two cases at the outputs O_2 are more deviant than other cases at O_1 and O_3. For example, with $\lambda > 1555$ nm, the I.L of TE_1 and TE_2 modes when switching to O_2 are better than other ones in terms of the wavelength response, especially for TE_2. This reason can be addressed by MMI_2 operating in the symmetric interference mechanism better than operating general interference mechanism in this wavelength range.

On the other hand, Cr.T has the best values within the wavelength range from 1545 nm to 1555 nm, from - 25 dB to - 32.5 dB, as seen in Fig. 7b. It also exhibits that Cr.T of the TE_1 mode to O_3 is the lowest in the wavelength range of 1550 nm to 1570 nm, expanding from - 23 dB to - 32.5 dB. On the contrary, the remaining cases fluctuate similarly with a small gap

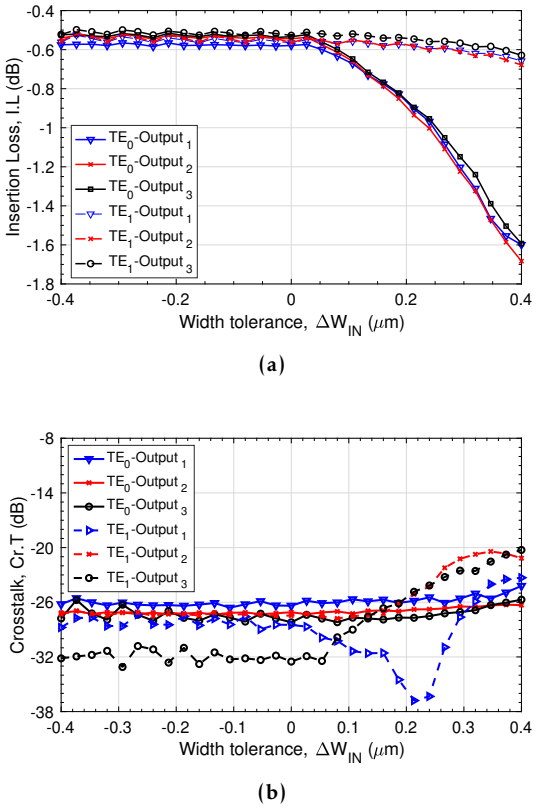

Figure 8. Insertion loss (a) and crosstalk (b) of the proposed switch as a function of the width tolerance.

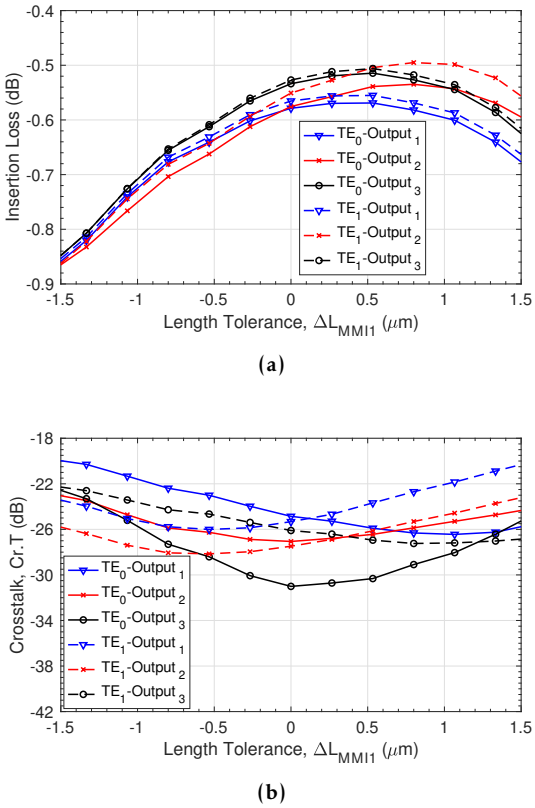

Figure 9. Insertion loss (a) and crosstalk (b) of the proposed switch as a function of the length tolerance of MMI_1.

from 3 dB to 4 dB and reach the highest value of - 19 dB. Such a good performance covering the whole C-band is a significant result for applications in short-haul optical communication systems and photonic integrated circuits [50, 51].

In order to characterize the functioning of the silicon device, evaluating the fabrication tolerances of the photonic devices is indispensable, especially, for a photonic design based on numerical simulations. Because, fabrication tolerances can come from computing algorithms of the simulation program, the resolution quality of the photolithography or electron beam lithography technologies using in the experimental manufacturing process, imperfect quality of the supplied SOI wafer, imperfect etching process, etc. Noted that, the larger fabrication tolerances are, the higher producibility can reach. In particular, it is well-known that MMI couplers typically have relatively large geometry tolerances because their widths are very large compared to typical single-mode access waveguides. Hence, in this paper, we only consider the fabrication tolerances of the device under the influence of geometrical parameters including the width of input-waveguide (W_{IN}), the length of MMI_1 (L_{MMI_1}), the length of MMI_2 (L_{MMI_2}), and the slab height layer (H_{S}) in the rib/ridge waveguide structure. The results investigated at the wavelength of 1550 nm are plotted correspondingly in Figs. 8 - 11.

The first one we can observe from Figs. 8b - 11b is that Cr.T of all cases is less than -19 dB to reach the acceptable values of device fabrication tolerances. In addition, it is interesting to see that the length tolerance of two MMI couplers is very close in the gap of [-1.5, 1.5]μm, as illustrated in Figs. (9, 10).

For the insertion loss cases, we inquire the similar impact of the length tolerances of L_{MMI} on I.L (Figs. 9a and 10a) like in the cases of wavelength behavior (Fig.7a) whereas the I.Ls of ΔW_{IN} (Fig. 8a) and of ΔH_{S} (Fig. 11a) are behaved differently. Particularly, I.L of the three paths of TE_1 mode in Fig. 8a keep a small fluctuation in the range from - 0.5 dB to - 0.67 dB with the width tolerance of $\Delta W_{\mathrm{IN}} \in [-0.4, 0.4]$ μm. Meanwhile, the transmissions for TE_0 mostly fluctuate in a small value around - 0.55 dB in the range of - 0.4 μm $< \Delta W_{\mathrm{IN}} <$ 0.05 μm, then drop quite quickly to -1.68 dB at $\Delta W_{\mathrm{IN}} = 0.4$ μm. Therefore, chosing the tolerance of $\Delta W_{\mathrm{IN}} = \pm$ 0.05 μm is entirely appropriate. In addition, Figs. 9a and 10a show the I.L extending from - 0.87 dB to - 0.5 dB within the length tolerances of 3 μm for L_{MMI_1} and L_{MMI_2}. They have the same variation trend following the wavelength response, especially in terms

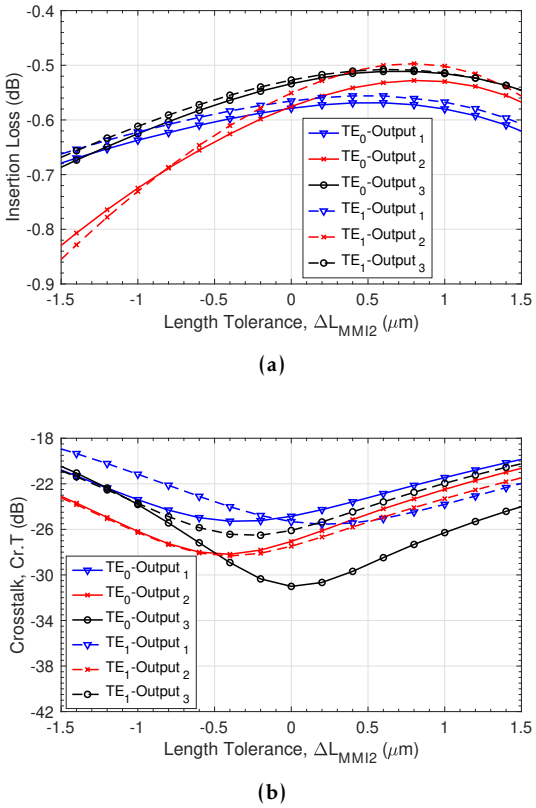

Figure 10. Insertion loss (a) and crosstalk (b) of the proposed switch as a function of the length tolerance of MMI_2.

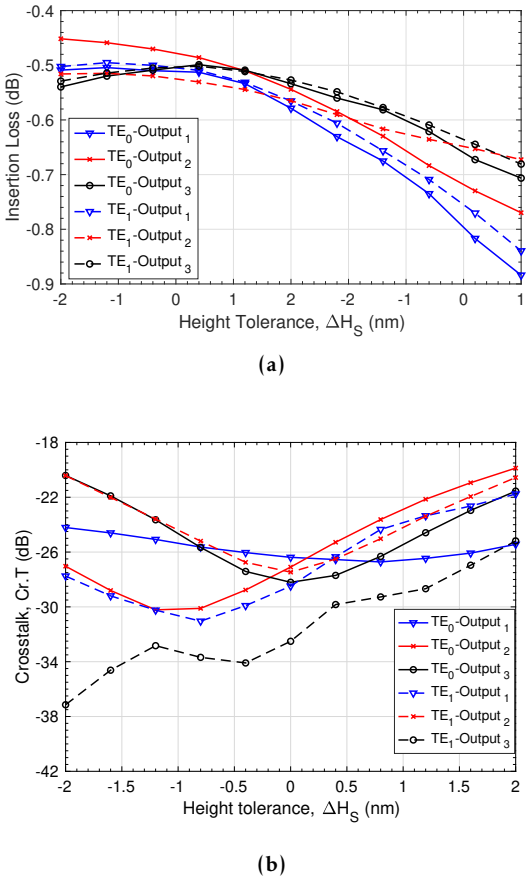

Figure 11. Insertion loss (a) and crosstalk (b) of the proposed switch as a function of the slab-height tolerance.

of both TE_0 and TE_1 modes at $Output_2$ of MMI_2. Finally, althought I.L and Cr.T are available in the ranges from - 0.88 dB to - 0.45 dB and - 37 dB to - 20 dB respectively, the tolerance of H_S in Fig. 11 is the smallest, about ± 2 nm. However, such a high requirement for height tolerances is completely able to attain by using current advanced fabrication techniques for very large scale integrated circuits (VLSI), such as 193-nm lithography [52].

4. Conclusion

This paper presented the design of a compact 1 × 3 two-mode selective router/switch constructed from a symmetrical Y-junction coupler and two MMI couplers based on the SOI platform through numerical simulations. The proposed device could well operate in the broad wavelength range from 1530 nm to 1570 nm with absolute values of insertion loss always smaller than 1 dB and crosstalk smaller than - 19 dB. Moreover, the estimated circuit footprint of the device was very compact, as small as 5 μm × 475 μm, and geometry tolerances were relatively large. Therefore, such an excellent property makes the proposed device strongly promising potential for applications in photonic integrated circuits as well as MDM-WDM systems.

Acknowledgment

The authors would like to thank Dr. Dao Duy Thang from Silicon Austria Labs for his advice and support on simulation tools of this research. This research was funded by Vingroup Innovation Foundation, Vin Bigdata by the Domestic PhD Scholarship Program, grant numbers VINIF.2019.TS.16 and VINIF.2020.TS.123

References

[1] D. Richardson, J. Fini, L. E. Nelson, Space-division multiplexing in optical fibres, Nature Photonics 7 (2013) 354–362.

[2] N. Bai, E. Ip, Y.-K. Huang, E. Mateo, F. Yaman, M.-J. Li, S. Bickham, S. Ten, J. L. nares, C. Montero, V. Moreno, X. Prieto, V. Tse, K. M. Chung, A. P. T. Lau, H.-Y. Tam, C. Lu, Y. Luo, G.-D. Peng, G. Li, T. Wang, Mode-division multiplexed transmission with inline few-mode fiber amplifier, Opt. Express 20 (2012) 2668–2680.

[3] D. Soma, S. Beppu, Y. Wakayama, K. Igarashi, T. Tsuritani, I. Morita, M. Suzuki, 257-tbit/s weakly coupled 10-mode c + l-band wdm transmission, Journal of Lightwave Technology 36 (2018) 1375–1381.
[4] R.-J. Essiambre, M. A. Mestre, R. Ryf, A. H. Gnauck, R. W. Tkach, A. R. Chraplyvy, Y. Sun, X. Jiang, R. Lingle, Experimental investigation of inter-modal four-wave mixing in few-mode fibers, IEEE Photonics Technology Letters 25 (6) (2013) 539–542.
[5] M. Ohashi, T. Kawasaki, H. Kubota, Y. Mivoshi, Prediction of modal dispersion of high-order mode from wavelength dependence of the mode field radius, in: 2019 24th OptoElectronics and Communications Conference (OECC) and 2019 International Conference on Photonics in Switching and Computing (PSC), IEEE, 2019, pp. 1–3.
[6] M. Jiang, C. Chen, B. Zhu, F. Hu, Mimo-free wdm–mdm bidirectional transmission over om3 mmf, Optics Communications 473 (2020) 125988.
[7] S. Chaudhary, A. Amphawan, High speed mdm-ro-fso communication system by incorporating ami scheme, International Journal of Electronics Letters 7 (3) (2019) 304–310.
[8] M. Jiang, C. Chen, B. Zhu, F. Hu, Mimo-free wdm–mdm bidirectional transmission over om3 mmf, Optics Communications 473 (2020) 125988.
[9] K. K. Upadhyay, N. K. Shukla, S. Chaudhary, A high speed 100 gbps mdm-sac-ocdma multimode transmission system for short haul communication, Optik 202 (2020) 163665.
[10] Z. Chen, Y. Zhu, X. Ruan, Y. Li, Y. Li, F. Zhang, Bridged coupler and oval mode converter based silicon mode division (de) multiplexer and terabit wdm-mdm system demonstration, Journal of Lightwave Technology 36 (13) (2018) 2757–2766.
[11] T. Masunda, A. Amphawan, Feedforward equalizers for mdm–wdm in multimode fiber interconnects, Journal of Optical Communications 39 (2) (2018) 147–153.
[12] C. Williams, G. Zhang, R. Priti, G. Cowan, O. Liboiron-Ladouceur, Modal crosstalk in silicon photonic multimode interconnects, Optics express 27 (20) (2019) 27712–27725.
[13] J. M. Lukens, A. Dezfooliyan, C. Langrock, M. M. Fejer, D. E. Leaird, A. M. Weiner, Demonstration of high-order dispersion cancellation with an ultrahigh-efficiency sum-frequency correlator, Physical review letters 111 (19) (2013) 193603.
[14] A. V. Bourdine, Method for chromatic dispersion estimation of high-order guided modes in graded index single-cladding fibers, in: Optical Technologies for Telecommunications 2006, Vol. 6605, International Society for Optics and Photonics, 2007, p. 660509.
[15] Y. Tong, W. Zhou, X. Wu, H. K. Tsang, Efficient mode multiplexer for few-mode fibers using integrated silicon-on-insulator waveguide grating coupler, IEEE Journal of Quantum Electronics 56 (1) (2019) 1–7.
[16] P.-C. Kuo, Y. Tong, C.-W. Chow, J.-F. Tsai, Y. Liu, Y.-C. Chang, C.-H. Yeh, H. K. Tsang, 4.36 tbit/s silicon chip-to-chip transmission via few-mode fiber (fmf) using 2d sub-wavelength grating couplers, in: Optical Fiber Communication Conference, Optical Society of America, 2021, pp. M3D–6.
[17] P. Guo, W. Hou, L. Guo, Z. Ning, M. S. Obaidat, W. Liu, Wdm-mdm silicon-based optical switching for data center networks, in: ICC 2019-2019 IEEE International Conference on Communications (ICC), IEEE, 2019, pp. 1–6.
[18] Y. Tan, H. Wu, D. Dai, Silicon-based hybrid (de)multiplexer for wavelength-/polarization-division-multiplexing, J. Light. Technol. 36 (2018) 2051–2058.
[19] D. Melati, A. Melloni, Integrated all-optical mimo demultiplexer for 8-channel mdm-wdm transmission, 2017 Conf. Lasers Electro-Optics Pacific Rim (2017) 1–4.
[20] C. D. Truong, T. H. Nguyen, Q. T. Pham, M. T. Trinh, K. Vu, Three-mode multiplexer and demultiplexer utilizing trident and multimode couplers, Optics Communications 435 (2019) 334–340.
[21] W. Jiang, J. Miao, T. Li, Compact silicon 10-mode multi/demultiplexer for hybrid mode- and polarisation-division multiplexing system, Sci. Rep. 9 (2019) 13223.
[22] D. Ge, J. Li, Z. Wu, F. Ren, P. Zhu, Q. Mo, Z. Li, Z. Chen, Y. He, Experimental demonstration of roadm functionalities for hybrid mdm-wdm optical networks, in: 2016 Optical Fiber Communications Conference and Exhibition (OFC), IEEE, 2016, pp. 1–3.
[23] N. P. Diamantopoulos, M. Hayashi, Y. Yoshida, A. Maruta, R. Maruyama, N. Kuwaki, K. Takenaga, H. Uemura, S. Matsuo, K.-I. Kitayama, Mode-unbundled roadm and bidirectional mode assignment for mdm metro area networks, Journal of Lightwave Technology 33 (2015) 5055–5061.
[24] H. Ye, F. Yu, Y. Liu, Z. Yu, J. Li, D. Zhu, B. Su, W. Xu, Ultra-compact waveguide-integrated te-mode converters with high mode purity by designing ge/si patterns, IEEE Photonics J 11.
[25] H. D. Tam Linh, T. C. Dung, K. Tanizawa, D. D. Thang, N. T. Hung, Arbitrary te0/te1/te2/te3 mode converter using 1×4 y-junction and 4×4 mmi couplers, IEEE J. Sel. Top. Quantum Electron 26 (2020) 8300708.
[26] H. Jia, T. Zhou, X. Fu, J. Ding, L. Zhang, L. Yang, Fourport mode-selective silicon optical router for on-chip optical interconnect, Opt. Express 26 (2018) 9740–9748.
[27] H. Jia, T. Zhou, X. Fu, J. Ding, L. Zhang, L. Yang, Integrated five-port non-blocking optical router based on mode-selective property, Nanophotonics 7 (2018) 853–858.
[28] B. Stern, X. Zhu, C. P. Chen, L. D. Tzuang, J. Cardenas, K. Bergman, M. Lipson, On-chip mode-division multiplexing switch, Optica 2 (2015) 530.
[29] R. B. Priti, O. Liboiron-Ladouceur, Reconfigurable and scalable multimode silicon photonics switch for energy efficient mode-division-multiplexing systems, J. Light. Technol 37 (2019) 530.
[30] H. Xiao, L. Deng, G. Zhao, Z. Liu, Y. Meng, X. Guo, G. Liu, S. Liu, J. Ding, Y. Tian, Optical mode switch based on multimode interference couplers, J. Opt. (United Kingdom) 19 (2017) 1–6.
[31] X. Han, Z. Zhang, J. Yang, H. Xiao, G. Ren, Y. Jiang, T. Zhao, T. G. Nguyen, A. Mitchell, J. Yang, Y. Tian, On-chip switchable and reconfigurable optical mode exchange device using cascaded three-waveguide-coupling switches, Express 28 (2020) 9552–9562.

[32] R. B. Priti, H. P. Bazargani, Y. Xiong, O. Liboiron-Ladouceur, Mode selecting switch using multimode interference for on-chip optical interconnects, Opt. Lett 42 (2017) 4131–4134.
[33] R. B. Priti, F. Shokraneh, O. Liboiron-Ladouceur, Scalable 2 × 2 multimode switch for mode- multiplexed silicon photonics interconnects, in Proc. 2018 Asia Communications and Photonics Conference (ACP) (2018) 1–3.
[34] A. Biberman, B. G. Lee, N. Sherwood-Droz, M. Lipson, K. Bergman, Broadband operation of nanophotonic router for silicon photonic networks-on-chip, IEEE Photonics Technol. Lett 22 (2010) 926–928.
[35] G. Calò, V. Petruzzelli, Compact design of photonic crystal ring resonator 2×2 routers as building blocks for photonic networks on chip, J. Opt. Soc. Am. B 31 (2014) 517–525.
[36] A. Crespo-Poveda, A. Cantarero, M. M. de Lima, Reconfigurable photonic routers based on multimode interference couplers, J. Opt. Soc. Am. B 33 pages = 81, year = 2016, doi = ,.
[37] A. Annoni, E. Guglielmi, M. Carminati, G. Ferrari, M. Sampietro, D. A. Miller, A. Melloni, F. Morichetti, Unscrambling light - automatically undoing strong mixing between modes, Light Sci. Appl 6 (2017) 1–10.
[38] C. Li, D. Liu, D. Dai, Multimode silicon photonics, Nanophotonics 8 (2018) 227–247.
[39] D. N. T. Hang, H. T. Duy, T. T. T. Thanh, N. D. H. Khoi, C. D. Truong, Compact, highly efficient, and controllable simultaneous 2× 2 three-mode silicon photonic switch in the continuum band, IEEE Access 9 (2021) 102387–102396.
[40] C. D. Truong, D. N. T. Hang, H. Chandrahalim, M. T. Trinh, On-chip silicon photonic controllable 2× 2 four-mode waveguide switch, Scientific Reports 11 (1) (2021) 1–14.
[41] B. J. Frey, et al., Temperature-dependent refractive index of silicon and germanium, Optomechanical Technologies for Astronomy 6273 (2006) 62732J.
[42] S. M. Eaton, M. L. Ng, R. Osellame, P. R. Herman, High refractive index contrast in fused silica waveguides by tightly focused, high-repetition rate femtosecond laser, Journal of Non-Crystalline Solids 357 (11-13) (2011) 2387–2391.
[43] S. Triki, M. Najjar, H. Rezig, 2d-bpm-eim technique for analyzing multilayer wdm demultiplexer based on rib waveguide, Journal of optical communications 30 (3) (2009) 136–138.
[44] J. D. Love, N. Riesen, Single-, few-, and multimode y-junctions, Journal of Lightwave Technology 30 (2012) 304 – 309.
[45] D.-X. Xu, J. H. Schmid, G. T. Reed, G. Z. Mashanovich, D. J. Thomson, M. Nedeljkovic, X. Chen, D. Van Thourhout, S. Keyvaninia, S. K. Selvaraja, Silicon photonic integration platform – have we found the sweet spot?, IEEE J. Sel. Top. Quantum Electron 20 4 (2014) 189–205.
[46] H. F. Taylor, Power loss at directional change in dielectric waveguides, Appl. Opt 13 (1974) 642–647.
[47] Y. A. Vlasov, S. J. McNab, Losses in single-mode silicon-on-insulator strip waveguides and bends, Optics express 12 (8) (2004) 1622–1631.
[48] L. Soldano, E. Pennings, Optical multi-mode interference devices based on self-imaging: Principles and applications, J. Light. Technol 13 (1995) 615–627.
[49] Álvaro Rosa, A. Gutiérrez, A. Brimont, A. Griol, P. Sanchis, High performace silicon 2x2 optical switch based on a thermo-optically tunable multimode interference coupler and efficient electrodes, Opt. Express 24 (2016) 191–198.
[50] C. Sun, Y. Yu, G. Chen, X. Zhang, Integrated switchable mode exchange for reconfigurable mode-multiplexing optical networks, Optics Letters 41 (2016) 3257–3260.
[51] X. Zi, L. Wang, K. Chen, K. S. Chiang, Mode-selective switch based on thermo-optic asymmetric directional coupler, IEEE Photonics Technol. Lett 30 (2018) 618–621.
[52] D. Bratton, D. Yang, J. Dai, C. K. Ober, Recent progress in high resolution lithography, Polymers for Advanced Technologies 17 (2) (2006) 94–103.